Contents lists available at ScienceDirect

International Journal of Heat and Mass Transfer

journal homepage: www.elsevier.com/locate/hmt



Features of transport in non-Gaussian random porous systems

Check

Felipe P.J. de Barros a,*, Alberto Guadagnini b, Monica Riva b

- ^a Sonny Astani Department of Civil and Environmental Engineering, University of Southern California, Kaprielian Hall, Room 224B 3620 S. Vermont Avenue, Los Angeles, CA 90089-2531, United States
- ^b Department of Civil and Environmental Engineering, Politecnico di Milano, Piazza L. Da Vinci, 32, Milan, 20133, Italy

ARTICLE INFO

Article history:
Received 20 May 2021
Revised 22 October 2021
Accepted 9 November 2021
Available online 21 November 2021

2010 MSC: 00-01 99-00

Keywords:
Flow and transport in porous media
Uncertainty quantification
Semi-analytical methods
Random flows
Probabilistic risk analysis
Solute transport
Environmental fluid mechanics

ABSTRACT

The goal of this work is to employ a semi-analytical framework to investigate key features associated with the transport behavior of an inert solute in non-Gaussian random fields. We focus our analysis on the transport dynamics of a solute plume through a porous medium characterized by spatially heterogeneous non-Gaussian log-conductivity fields, Y. We rest on a stochastic Lagrangian framework to provide semi-analytical formulations to evaluate the statistical moments and cumulative distribution function (CDF) of solute concentration. The heterogeneous structure of the log-conductivity field is modeled as a Generalized Sub-Gaussian process. This model has been shown to capture non-Gaussian and scale-dependent features displayed by several variables, including key parameters of porous media. Our results suggest that the effects of non-Gaussianity in Y on solute concentrations statistics are more pronounced at locations near the solute source zone and at early times. The impact of the analyzed non-Gaussian nature of the field of Y is also significant at the lower tails of the distribution. We also explore conditions under which when the concentration CDF in Generalized Sub-Gaussian Y fields can be approximated by the widely used beta distribution. Furthermore, the methodology used in this work is an alternative to the commonly used numerical Monte Carlo method and can be employed as a benchmark tool in computational stochastic mass transport problems in porous media.

© 2021 Elsevier Ltd. All rights reserved.

1. Introduction

Capturing the effects of spatial heterogeneity on transport of dissolved chemicals in porous media is key to a variety of Earth science and engineering scenarios including, e.g., effective allocation of subsurface water and energy resources, reservoir engineering, environmental risk assessment for contaminated groundwater bodies, or safety assessment of hazardous waste facilities. Spatial and temporal patterns of a solute plume migrating across a porous material are essentially driven by two elements: (a) the interplay between advective and diffusive mass fluxes and (b) the spatial disorder of the porous medium. At a continuum scale, the latter can be described through the spatial heterogeneity of properties/attributes that characterize the medium. Amongst these, hydraulic conductivity is recognized to display spatial heterogeneity over a multitude of scales. The ensuing spatial heterogeneity of fluid flow leads to solute transport being associated with anomalous dispersion features. The latter are related to a non-linear tem-

E-mail address: fbarros@usc.edu (F.P.J. de Barros).

poral evolution of solute particle displacement distribution as well as heavy-tailed first-passage time distributions [1,2]. Medium properties are typically characterized in a stochastic context due to our inability to fully capture the details of their spatial variability [3]. Hence, state variables such as solute fluxes and concentrations are also interpreted as random quantities.

Space-time evolution of concentration mean and variance in porous media characterized by a heterogeneous distribution of hydraulic conductivity have been subject to extensive studies, e.g., [3-8]. Analytical investigations are generally relying on perturbation theory and consider the (natural) logarithm of conductivity to form a multi-Gaussian random field [7,9,10]. The appraisal of the full probability distribution of concentration at a given point in space and time has also been subject of investigation. Based on the results obtained from turbulent flow studies [11,12], numerical analyses performed on synthetic random conductivity fields [13-17] suggest that a beta-distribution could be adopted as a model to describe the probability distribution of concentrations in a spatially heterogeneous flow field. Alternative approaches yielding the full probability density function of concentrations are also reported [18-23]. The coupled effects of natural heterogeneity and engineered devices (i.e. sampling volume and solute injection source

^{*} Corresponding author.

zones) were also semi-analytically quantified on the concentration probability density function, PDF, in two and three dimensional flows [22]. Most of these works rely on the assumption that the log-conductivity field can be described through a Gaussian distribution. Studies have shown that non-Gaussian features could have an impact on hydraulic connectivity and therefore solute dispersion [24–26]. In this framework, a key element which we address in this study (and has not yet been completely explored) is the significance that documented scale-dependence and non-Gaussian features of the probability distribution of log-conductivity can have on the characterization of the uncertainty associated with solute concentrations.

The main motivation underlying our work is related to the mounting evidences that probability distributions and associated statistical moments of a variety of geophysical and environmental variables (as well as their spatial increments) display distinctive scale-dependent features. Typical manifestations of scaling behavior we consider here are those displayed by the increments of a given variable, Y. These include (a) evidences that characteristic features of the probability distributions of the increments of Y vary with the separation distance (or lag) between pairs of points at which such increments are evaluated [27], and (b) the documented Extended Self-Similarity (ESS) displayed in several cases by *q*-order structure functions associated with such increments [28-30]. Observations indicate that (a) increment distributions appear to be symmetric, with peaks that become higher and tails that become heavier as the lag decreases, and (b) the shape of the increment distribution tends to transition towards Gaussian as lag increases. Environmental variables displaying such a behavior, and directly related to our study, include log-hydraulic conductivity and permeability [27,30-36], log-air permeability [37], electrical resistivity [38,39], vadose zone hydraulic properties [40], neutron porosity [41], sediment transport [42], and micro-scale geochemical data related to surface topography of calcite crystals [43].

Riva et al. [41,44] introduced a modeling framework based on a Generalized Sub-Gaussian (GSG) process that embeds the above empirical documentations of statistical scaling. In essence, the GSG model allows representing jointly, within a unique framework, all of the above-documented scaling manifestations (as described for probability distributions and/or structure functions) of a quantity and its two-point incremental values through the action of a (spatially uncorrelated) subordinator on an otherwise spatially correlated Gaussian random field. To date, this modeling strategy has been successfully applied to the interpretation of main features displayed by key parameters of porous media, including logpermeability and porosity [27,41,43], whose spatial heterogeneity is typical of natural subsurface settings. It has also been employed in preliminary analytical and numerical studies of flow and transport in porous media whose log-conductivity is characterized through a GSG model [45,46].

In the present contribution, we aim at examining key elements of the uncertainty related to concentration fields evolving through log-conductivity fields displaying scaling features described by the GSG model. Through the use of a semi-analytical framework, we show how such non-Gaussian features control the mean, standard deviation and cumulative distribution function, CDF, of resident concentration at various downstream locations from a source where solute is injected in the system. Given the environmental relevance of extreme values, we emphasize the way such non-Gaussian features impact the tailing behavior of concentration distributions. In addition to being an alternative computational method in itself, the proposed approach is well-suited for benchmarking purposes. Although the focus of our study lies on mass transfer, the method of analysis is directly applicable to problems in heat transfer in randomly heterogeneous porous media.

2. Problem formulation

We study transport of an inert solute in a steady-state flow field taking place across a two-dimensional (2D) porous medium in the absence of sources and sinks and far from boundaries, so that boundary effects are negligible. The system is characterized by a spatially heterogeneous (locally isotropic) hydraulic conductivity $K(\mathbf{x})$ and uniform porosity ϕ , $\mathbf{x} = (x_1, x_2)^T$ corresponding to a Cartesian coordinate system. As a result of the spatial variability of K, the flow field is also spatially heterogeneous. Steady-state flow is governed by

$$\nabla \cdot \mathbf{q}(\mathbf{x}) = 0, \tag{1}$$

with $\mathbf{q}(\mathbf{x})$ denoting the Darcy flux. The spatially heterogeneous K-field of the medium can be mapped onto the divergence free flow field through Darcy's law

$$\mathbf{q}(\mathbf{x}) = -K(\mathbf{x})\nabla h(\mathbf{x}),\tag{2}$$

where $h(\mathbf{x})$ corresponds to the hydraulic head. Velocity $\mathbf{v}(\mathbf{x})$ is given by $\mathbf{q}(\mathbf{x})/\phi$. Given the physical setup, the flow field is uniform-in-the-mean along the longitudinal, x_1 , direction with mean velocity $\langle \mathbf{v}(\mathbf{x}) \rangle = (V_1, 0)^T$. Here the angled brackets denotes ensemble expectation and $V_1 = K_G \mathcal{J}/\phi$ with K_G representing the geometric mean of the conductivity field, and $\mathcal{J} = -\partial \langle h(\mathbf{x}) \rangle / \partial x_1$.

An inert solute is instantaneously released into the flow domain over a rectangular injection area $S_0 = \ell_1 \times \ell_2$ where ℓ_i is the size of source zone along the i^{th} -direction. The resident concentration $c(\mathbf{x},t)$ satisfies the advection-dispersion equation

$$\frac{\partial c(\mathbf{x}, t)}{\partial t} + \mathbf{v}(\mathbf{x}) \cdot \nabla c(\mathbf{x}, t) = D\nabla^2 c(\mathbf{x}, t), \tag{3}$$

where D denotes the local-scale dispersion coefficient, taken here as a constant. Analytical solutions for the advection-dispersion Eq. (3) under uniform flow conditions, i.e. constant \mathbf{v} , and different coordinate systems are available in the literature [e.g., 47, 48, and references therein]. In this work, we account for the effects of the spatial random fluctuations of \mathbf{v} on the stochastic characterization of c. The initial condition, corresponding to an instantaneous injection of the solute, is taken as

$$c(\mathbf{x},0) = \begin{cases} C_0 & \text{if } \mathbf{x} \in \mathcal{S}_0 \\ 0 & \text{if } \mathbf{x} \notin \mathcal{S}_0, \end{cases}$$
 (4)

where C_0 is the initial concentration of the injected solute mass, which is taken as constant.

3. Methods

3.1. Random space function model

Let $Y(\mathbf{x})$ denote the log-conductivity field, i.e. $Y(\mathbf{x}) = \ln K(\mathbf{x})$. We pattern $Y(\mathbf{x})$ through the Generalized Sub-Gaussian (GSG) model [41,44], i.e.,

$$Y(\mathbf{x}) = \mathcal{U}(\mathbf{x})\mathcal{G}(\mathbf{x}). \tag{5}$$

Here, $\mathcal{G}(\mathbf{x})$ represents a Gaussian random field whilst $\mathcal{U}(\mathbf{x})$ is a subordinator that is independent of $\mathcal{G}(\mathbf{x})$. As shown in Riva et al. [41,44], $\mathcal{U}(\mathbf{x})$ consists of statistically independent identically distributed positive random variables at all points of the domain. For this work, we take $\mathcal{G}(\mathbf{x})$ as a statistically homogeneous and isotropic Gaussian random field characterized by an isotropic exponential covariance function (other choices being compatible with the GSG model), namely $\sigma_G^2 \exp[-r/I_G]$, with variance σ_G^2 and integral scale I_G , and $r = |\mathbf{x} - \mathbf{x}'|$ denoting the lag-distance. The variance and integral scale of $Y(\mathbf{x})$ are given respectively by $\sigma_Y^2 = \langle \mathcal{U}^2 \rangle \sigma_G^2$ and $I_Y = I_G/\eta$, with $\eta = \langle \mathcal{U}^2 \rangle / \langle \mathcal{U} \rangle^2$, while the (isotropic) covariance of $Y(\mathbf{x})$ is defined as

$$C_Y(r) = \langle \mathcal{U} \rangle^2 \sigma_G^2 e^{-r/I_G}, \text{ for } r > 0.$$
 (6)

Note that whereas for $\mathcal{G}(\mathbf{x})$ the variance and covariance coincide at r = 0, the sub-Gaussian field $Y(\mathbf{x})$ exhibits a nugget effect. The reader is referred to Riva et al. [41] for additional details. The spectral representation Eq. (6) is

$$\hat{C}_{Y}(\mathbf{k}) = \langle \mathcal{U} \rangle^{2} \sigma_{G}^{2} I_{G}^{2} \frac{1}{(1 + k^{2} \eta^{2} I_{V}^{2})^{3/2}}, \tag{7}$$

or equivalently

$$\hat{C}_{Y}(\mathbf{k}) = \eta \sigma_{Y}^{2} l_{Y}^{2} \frac{1}{(1 + k^{2} \eta^{2} l_{V}^{2})^{3/2}},$$
(8)

where **k** is the wave number vector. When $\eta = 1$, Eq. (8) reduces to the spectral representation of a multi-Gaussian log-conductivity field characterized by an exponential covariance function [3].

Under the assumptions listed in this work (i.e., 2D uniform-in-the-mean flow and negligible boundary effects), for low-to-mild levels of heterogeneity (i.e. $\sigma_Y^2 \lesssim 1$), the first-order solution of the Fourier transform of the velocity covariance function is given by Gelhar and Axness [49] and Dagan [50]

$$\hat{v}_{ij}(\mathbf{k}) = V_1^2 \left[\delta_{1i} - \frac{k_i k_1}{k^2} \right] \left[\delta_{1j} - \frac{k_j k_1}{k^2} \right] \hat{C}_Y(\mathbf{k}), \quad \text{for} \quad i, \ j = 1, 2 \quad (9)$$

where δ_{ii} is the Kronecker delta.

3.2. Uncertainty quantification of the concentration field

3.2.1. Low-order moments

In order to evaluate the statistics of solute concentration in a heterogeneous $Y(\mathbf{x})$ field, we cast our work within a Lagrangian framework [7,50]. The injection area $S_0 = \ell_1 \times \ell_2$ can be considered as a collection of solute particles, each traveling along a specific pathline across the heterogeneous system. The trajectory evaluated at time t for the particle released at location $\mathbf{a} = (a_1, a_2)^T$, denoted by $\mathbf{X}(t; \mathbf{a})$, is a function of the random spatial structure of the Y-field. As a consequence, solute pathlines are also random. Making use of the Lagrangian framework, solute concentration $c(\mathbf{x}, t)$ in Eq. (3) can be expressed as

$$c(\mathbf{x},t) = C_0 \int_{S_0} \delta[\mathbf{x} - \mathbf{X}(t;\mathbf{a})] d\mathbf{a}, \tag{10}$$

where δ is the Dirac's delta function.

We recall that the mean particle displacement is given by $\langle \mathbf{X}(t;\mathbf{a}) \rangle = \mathbf{a} + \langle \mathbf{v}(\mathbf{x}) \rangle t$ and, considering a first-order (in σ_Y^2) approximation theory, the advective and diffusive displacements can be assumed to be statistically independent [7]. We further note that, as travel time progresses (i.e., considering large travel distances in terms of I_Y) trajectory fluctuations, $\mathbf{X}'(t;\mathbf{a}) = \mathbf{X}(t;\mathbf{a}) - \langle \mathbf{X}(t;\mathbf{a}) \rangle$, tend to become Gaussian (by virtue of the central limit theorem). Introducing the one-particle, $X_{ii}(t) = \langle (X_i'(t;\mathbf{a}))^2 \rangle$, and the two-particles $Z_{ii}(t;\mathbf{a}-\mathbf{b}) = \langle X_i'(t;\mathbf{a})X_i'(t;\mathbf{b}) \rangle$ trajectory covariance functions, Fiori and Dagan [7] show that, if the injection zone is small compared to the characteristic length scale of heterogeneity (i.e., $\ell_i < I_Y$ and $Z_{ii}(t;\mathbf{a}-\mathbf{b}) \cong Z_{ii}(t;0)$), the mean, $\langle c(\mathbf{x},t) \rangle$, and variance, $\sigma_c^2(\mathbf{x},t)$, of $c(\mathbf{x},t)$ can be evaluated as

$$\langle c(\mathbf{x},t)\rangle = C_0 \prod_{i=1}^{2} \frac{1}{2} \left\{ \operatorname{erf} \left[\frac{x_i - V_i t + \ell_i / 2}{\sqrt{2X_{ii}(t)}} \right] - \operatorname{erf} \left[\frac{x_i - V_i t - \ell_i / 2}{\sqrt{2X_{ii}(t)}} \right] \right\},$$
(11)

$$\sigma_c^2(\mathbf{x},t) = C_o^2 \prod_{i=1}^2 \int_{-\ell_i/2}^{\ell_i/2} \Theta(x_i; a_i) da_i - \langle c(\mathbf{x}, t) \rangle^2, \tag{12}$$

where the function $\Theta(x_i; a_i)$ is defined as

$$\Theta(x_i; a_i) = \frac{\text{erf}[\mathcal{A}(t; a_i)] - \text{erf}[\mathcal{B}(t; a_i)]}{2\sqrt{2\pi X_{ii}(t)}} e^{-\frac{(x_i - a_i - V_i t)^2}{2X_{ii}(t)}}$$
(13)

with

$$A(t; a_i) = \frac{\ell_i + (x_i - V_i t)(1 - \rho_{ii}(t) + a_i \rho_{ii}(t))}{\sqrt{2X_{ii}(t)(1 - \rho_{ii}(t)^2)}}$$
(14)

$$\mathcal{B}(t; a_i) = \frac{-\ell_i + (x_i - V_i t)(1 - \rho_{ii}(t) + a_i \rho_{ii}(t))}{\sqrt{2X_{ii}(t)(1 - \rho_{ii}(t)^2)}}.$$
 (15)

Here $\rho_{ii}(t) = Z_{ii}(t;0)/X_{ii}(t)$. Semi-analytical expressions for X_{ii} and Z_{ii} are provided in the Appendix (see Eqs. (A.2) and (A.6)) as functions of the Fourier transform of the velocity covariance function $\hat{v}_{ij}(\mathbf{k})$ defined by Eq. (9).

3.2.2. Cumulative distribution function

Next we compute the cumulative distribution function (CDF) of $c(\mathbf{x},t)$ following the framework developed in de Barros and Fiori [22]. The methodology relies on evaluating the concentration in a moving coordinate system, $\boldsymbol{\xi}$, set along the trajectory of the solute plume's centroid, $\chi(t;\mathbf{a}_0)$ where \mathbf{a}_0 is the centroid's position at initial time. Then $\boldsymbol{\xi} = \mathbf{x} - \chi(t;\mathbf{a}_0)$ and Eq. (10) can be written as

$$c(\boldsymbol{\xi},t) = C_0 \int_{S_0} \delta[\boldsymbol{\xi} - \mathbf{W}(t; \mathbf{a}, \mathbf{a}_0)] d\mathbf{a}, \tag{16}$$

where $\mathbf{W}(t; \mathbf{a}, \mathbf{a}_0) = \mathbf{X}(t; \mathbf{a}) - \mathbf{\chi}(t; \mathbf{a}_0)$ is the separation distance at time t between the trajectories of solute particles released at \mathbf{a} and \mathbf{a}_0 . Computing the concentration in terms of \mathbf{W} in lieu of \mathbf{X} allows filtering out the uncertainty of the trajectory of the solute plume centroid [13,22]. At first-order in σ_Y^2 , mean and variance of \mathbf{W} can be computed as [13]

$$\langle \mathbf{W}(t; \mathbf{a}, \mathbf{a}_0) \rangle = \mathbf{a} - \mathbf{a}_0$$

 $W_{ij}(t; \mathbf{a}, \mathbf{a}_0) = X_{ij}(t) + 2Dt - 2Z_{ij}(t; \mathbf{a} - \mathbf{a}_0) + Z_{ij}(t; 0),$ (17)

where X_{ij} and Z_{ij} are given by Eqs. (A.2) and (A.6), respectively. Since, we have assumed that the injection zone is small compared to the characteristic length scale of heterogeneity (see also the previous Section 3.2.1), Eq. (17) reduces to de Barros and Fiori [22]

$$\langle \mathbf{W}(t; \mathbf{a}, \mathbf{a}_0) \rangle \approx 0$$

 $W_{ij}(t; \mathbf{a}, \mathbf{a}_0) \approx X_{ij}(t) + 2Dt - Z_{ij}(t; 0).$ (18)

From Eq. (16) one can evaluate the statistical moments of $c(\xi,t)$. It has been shown that the variance of $c(\xi,t)$ vanishes for a finite Péclet and small injection zones (see, e.g., [13]). Therefore, $\langle c(\xi,t)\rangle \approx c(\xi,t)$ and Eq. (16) reduces to

$$c(\boldsymbol{\xi},t) = C_0 \int_{\mathcal{S}} p_W(\boldsymbol{\xi};t,\mathbf{a}) d\mathbf{a}, \tag{19}$$

where p_W is the probability density function, PDF, of **W**. Making use of Eq. (18) and assuming **W** to be normally distributed (see also the previous Section 3.2.1) yields

$$c(\xi, t) = C_0 \prod_{i=1}^{2} \frac{1}{2} \left\{ \text{erf} \left[\frac{\xi_i + \ell_i / 2}{\sqrt{2W_{ii}(t)}} \right] - \text{erf} \left[\frac{\xi_i - \ell_i / 2}{\sqrt{2W_{ii}(t)}} \right] \right\}.$$
 (20)

The approach described above has been also used to quantify the mixing of solutes in natural porous media displaying a uni-modal covariance function [51] and in hierarchical and multi-scale sedimentary architecture [52].

Finally the concentration CDF, $P_C(c^*; \mathbf{x}, t) \equiv \operatorname{Prob}[c(\mathbf{x}, t) \leq c^*]$, can be obtained by switching the coordinate system from $\boldsymbol{\xi}$ to \mathbf{x} . That implies that P_C depends on the PDF of $\boldsymbol{\chi}$, i.e. p_{χ} . The latter, for small plume sizes, has been shown to be Gaussian and characterized by mean equal to $\langle \mathbf{v}(\mathbf{x}) \rangle t$ and variance approximately equal to $Z_{ii}(t;0)$ [13,22,51,53]. Then, following Mood et al. [54], $P_C(c^*;\mathbf{x},t)$ is evaluated as

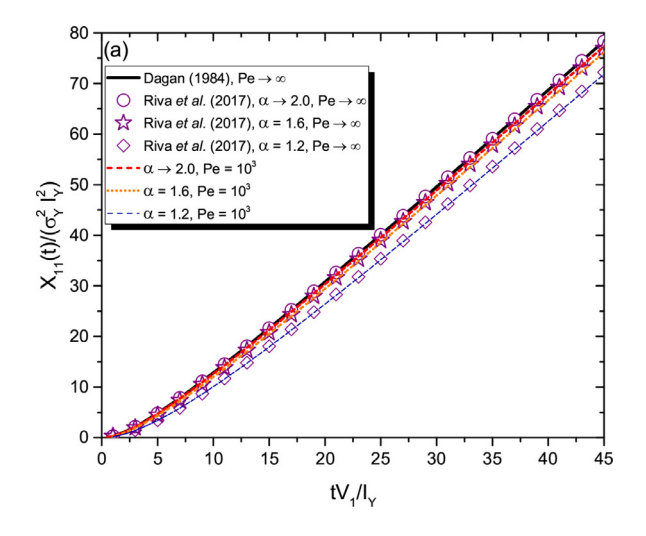
$$P_{\mathcal{C}}(c^*; \mathbf{x}, t) = \int_{\mathcal{D}_{\mathcal{C}}} p_{\chi}(\mathbf{\chi}; t) d\mathbf{\chi}. \tag{21}$$

The integration domain \mathcal{D}_C corresponds to the area of the χ_i (for i=1,2) space such that $c(\chi,t) \leq c^*$, therefore \mathcal{D}_C in Eq. (21) is determined by using Eq. (20). Evaluation of Eq. (21) constitutes the key step within a probabilistic environmental risk assessment framework, since it allows to quantify the probability that a contaminant concentration is below a threshold, c^* , fixed, e.g., by government or by environmental national/international agencies.

4. Results and discussion

For the purpose of illustration, we quantify solute concentration uncertainty in GSG fields by considering that the subordinator $\mathcal{U}(\mathbf{x})$ in Eq. (5) is lognormally distributed at every point \mathbf{x} with zero mean and variance $(2-\alpha)^2$, i.e. $\eta=\exp[(2-\alpha)^2]$ in Eqs. (7) and (8). When $\alpha\to 2$, $\eta=1$ and the log-conductivity field becomes Gaussian. As α decreases, the PDF of $Y(\mathbf{x})$ deviates from Gaussianity, exhibiting long tails and sharp peaks. In the following, we analyze the impact of the non-Gaussian nature of $Y(\mathbf{x})$ by varying α while maintaining a constant value for the variance, σ_Y^2 , and integral scale, I_Y , of $Y(\mathbf{x})$.

Fig. 1 depicts the temporal behavior of the one-particle trajectory covariance function for three values of α (decreasing from 2 to 1.2) and for a fixed Péclet number, defined as Pe = V_1I_Y/D . Here



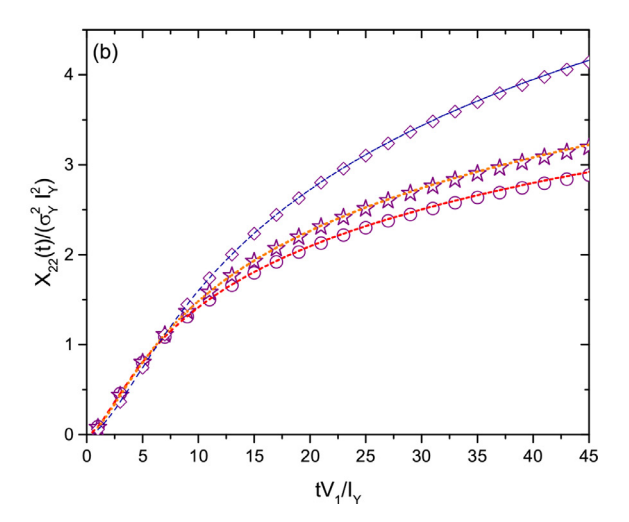
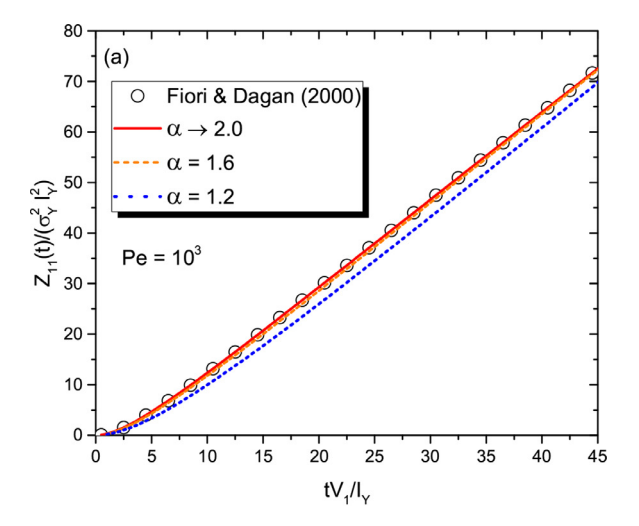


Fig. 1. Temporal evolution of the one-particle trajectory covariance function. Comparison with the results reported in Dagan [50] (for multi-Gaussian log-conductivity random fields) and Riva et al. [45].



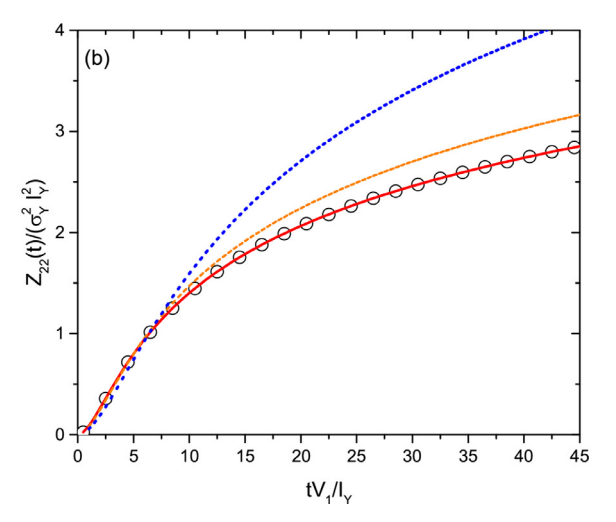


Fig. 2. Temporal evolution of the two-particle trajectory covariance function for Pe = 1000 and various values of α . Comparison with the results reported in Fiori and Dagan [7] for a multi-Gaussian log-conductivity random field.

we set Pe = 10^3 , this condition being characteristic of an advective dominated transport. Results are displayed along the longitudinal (Fig. 1a) and transverse (Fig. 1b) directions. The results of X_{ii} are compared with those obtained from the literature for Gaussian [50] and non-Gaussian [45] random flow fields under purely advective conditions, i.e., Pe $\rightarrow \infty$. As shown in Fig. 1, our results are in good agreement with those previously reported [45,50]. A similar comparison is performed in Fig. 2 for the two-particle trajectory covariance function.

Fig. 1 a shows that the longitudinal solute spreading decreases as the Y-field departs from a Gaussian behavior. This feature is linked to the spatial structure of the GSG fields of Y. We start by noticing that all of the results embedded in Fig. 1 are related to ensembles of Y-fields characterized by the same variance and integral scale. However, due to the shape of C_Y , the correlation of $Y(\mathbf{x})$ at small lags (local correlation) decreases with α (whereas the opposite occurs at large lags). Therefore, following the displacement of a particle along the mean flow direction, at a given time, the solute particle will have experienced (within each realization of the ensemble) a larger variability of Y-values at a low value of α (i.e., as the Y-field deviates from the Gaussian one) as compared to the heterogeneity experienced by a particle at larger α values (approaching the Gaussian case). As such, and recalling

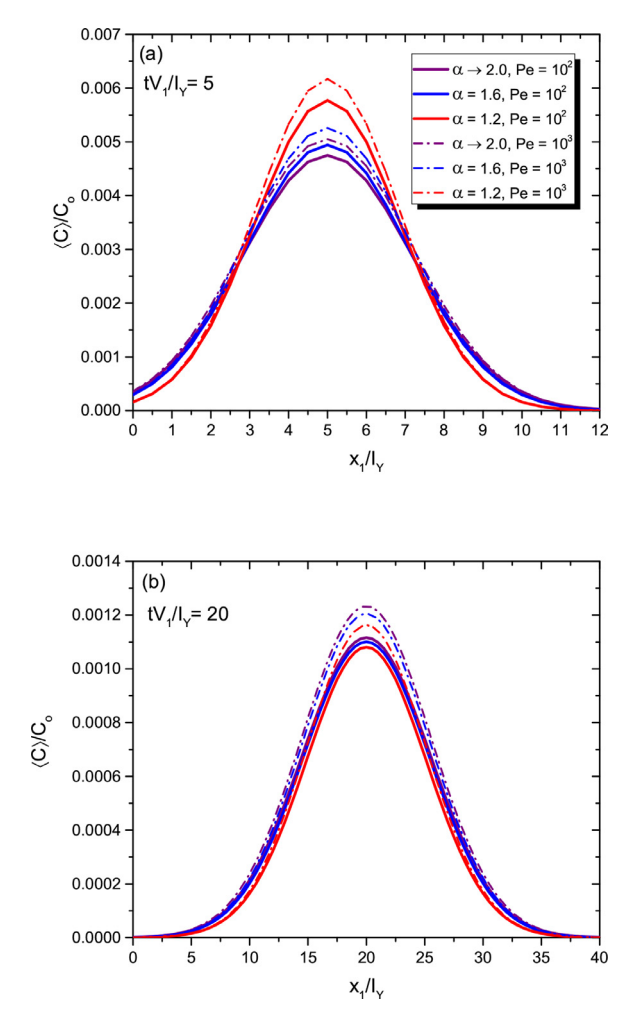
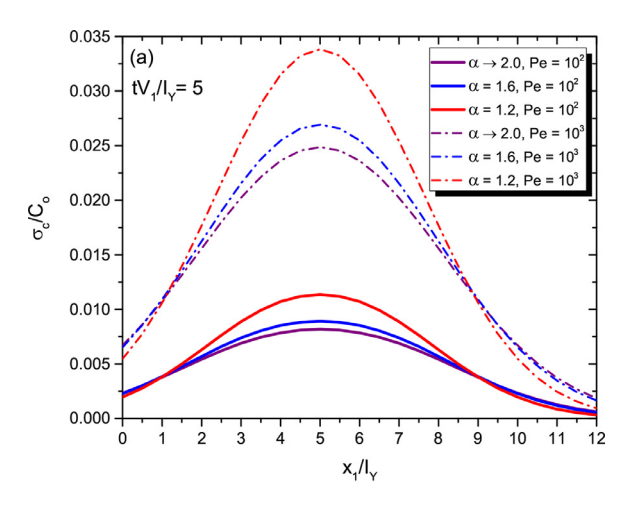


Fig. 3. Mean of *C* versus dimensionless longitudinal mean displacement $(x_2/l_Y=0)$, for selected values of Pe and α . Results are depicted for (a) early time $tV_1/l_Y=5$ and (b) late time $tV_1/l_Y=20$.

that $\sigma_{\rm v}^2$ is constant within each ensemble, the variability of the longitudinal displacement across the ensemble decreases as α decreases, as quantified by Fig. 1a. Otherwise, the transverse solute spreading decreases with α only for small travel distances, otherwise the situation is reversed (see Fig. 1b). Again, this feature is due to the structure of the GSG fields. For small values of α , in each realization of the ensemble, particles deviate more from the mean flow direction with respect to what observed for large α values (which are characterized by a larger level of local correlation, i.e., they are locally more homogeneous), resulting in larger X_{22} in the former than in the latter case. This result is consistent with the findings of Riva and Willmann [55] who analyzed the impact of the variogram structure (using exponential, spherical and Gaussian spatial correlation models) on the moments of transport observables in Gaussian Y fields under mean uniform and radial flow conditions by means of numerical Monte Carlo simulations. These authors show (see Fig. 7a in Riva and Willmann [55]) that the Gaussian variogram model displays the largest values of X_{22} at very small distances from the release point. Otherwise, the use of the exponential variogram (which is associated with the Y-field characterized by the smallest local correlation among those analyzed) results in the largest values of X_{22} . The results depicted in Fig. 2 for the two-particle trajectory covariance function are consistent with such findings. When $\alpha \rightarrow 2$, the computed values of Z_{ii} match those obtained by Fiori and Dagan [7] for a multi-Gaussian Y field. We highlight that non-locality (in the transport behavior)



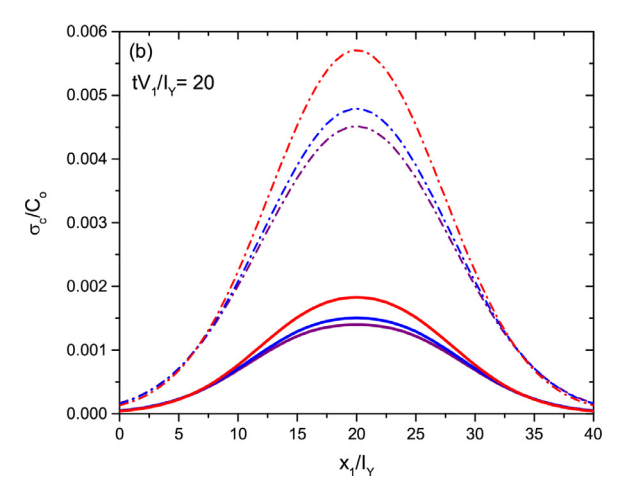


Fig. 4. Standard deviation of C versus dimensionless longitudinal mean displacement $(x_2/I_Y = 0)$, for selected values of Pe and α . Results are depicted for (a) early time $tV_1/I_Y = 5$ and (b) late time $tV_1/I_Y = 20$.

is reflected in the temporal dynamics of the one- and two-particle trajectory covariances as depicted in Figs. 1 and 2, where one can appreciate the impact of deviation from a Gaussian behavior of the underlying random conductivity field.

Next, we compute the spatial distribution of the mean, $\langle c(\mathbf{x},t) \rangle$, and standard deviation, $\sigma_c(\mathbf{x},t)$, of $c(\mathbf{x},t)$ at two dimensionless times, i.e., $tV_1/I_Y = 5$ and 20, and for three values of α (Figs. 3 and 4). Results are reported for $Pe = 10^2$ and 10^3 . These Pe numbers represent typical values observed in real aquifers. For example, a value of Pe = 380 has been inferred from concentration data monitored at the Cape Cod (Massachusetts, USA) experimental site [51,56]. We observe that the highest peak values for $\langle c(\mathbf{x},t) \rangle$ are related to the lowest values of α (Fig. 3a). This result is a reflection of the reduced spreading observed when the Y-field departs from the Gaussian behavior. Concentration uncertainty, as quantifies by its standard deviation (see Fig. 4), is also higher for small α values, as compared to the results for the Gaussian field (i.e. $\alpha \rightarrow 2$). As the log-conductivity field departs from Gaussianity (maintaining a constant variance and integral scale), each realization of the ensemble appears to be formed by larger zones displaying similar conductivity values and hot-spots of low/high conductivity values. This characteristic enhances the ensemble variability (i.e., large values of σ_C) and leads to a decreased solute spreading. As expected, the difference between statistics of $c(\mathbf{x},t)$ obtained with diverse α values decreases as the travel time increases and as Pe decreases

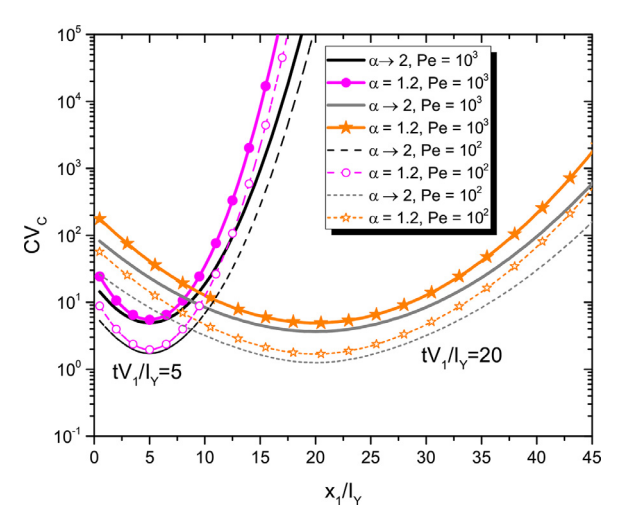
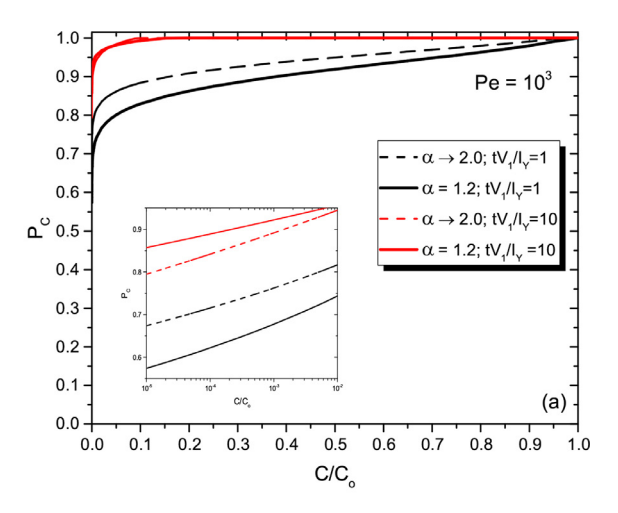


Fig. 5. Coefficient of variation of C versus dimensionless longitudinal mean displacement $(x_2/I_Y=0)$, for selected values of Pe and α .

(see also Fig. 3b). We point out that the effect of α on the concentration breakthrough curve (BTC) in a single realization of the permeability field has been investigated in the past [46,57]. In general, the authors observed that decreasing the value of α yields (i) a delayed first time of arrival of the solute and (ii) an increasing degree of asymmetry (and heavier tails) of the BTC.

The spatial distribution of the coefficient of variation of $c(\mathbf{x},t)$, defined as $CV_c = \sigma_c/\langle c \rangle$, is depicted in Fig. 5. Results are shown for different Pe and two dimensionless times and α values. In accordance to the results shown in Figs. 3 and 4, CV_c decreases as α increases and as Pe decreases. The minimum value of CV_c is observed at the average plume displacement, i.e. at $x_1/(tV_1) = 1$.

Concentration CDFs, $P_C(c^*; \mathbf{x}, t)$, are illustrated for the following cases: (i) position $\mathbf{x}/I_Y = (1, 0)^T$ and dimensionless time 1 and (ii) $\mathbf{x}/l_{Y} = (10, 0)^{T}$ and dimensionless time 10 for Pe = 10^{3} (Fig. 6a) and Pe = 10^2 (Fig. 6b). Both cases corresponds to $x_1/(tV_1) = 1$, i.e. P_C is evaluated along the average plume displacement. Close inspection of Fig. 6 reveals that the impact of α on P_C decreases as the travel distance increases. On the other hand, we observe marked differences at the low-concentration tail of the CDFs (as shown in the insets of Fig. 6) for all values of Pe and travel times explored. In particular, for low c^* , P_C increases with α for short travel distances from the source (a result which is in agreement with the numerical simulations of Libera et al. [46]), this behavior being otherwise reversed (compare values of P_C for different α at dimensionless times 1 and 10). This aspect is of particular relevance within a probabilistic risk (health or environmental) assessment framework, where c^* coincides with a maximum contaminant level for human or environmental health. To further elucidate this element, Fig. 7 depicts the probability of concentration exceeding the normalized threshold $c^* = 10^{-3}$, i.e., $1-P_C(c^*)$, versus α evaluated along the average plume displacement at various (dimensionless) times for the two values of Pe considered. At early times, the probability of exceeding the target threshold increases as the Y-field deviates from the Gaussian behavior. The opposite is seen to occur at late times. Fig. 8 provides a three-dimensional view of the dependence of exceedance probability on dimensionless time and α for the two distinct Péclet numbers analyzed. These results evidence that representing log-conductivity through a GSG model can have a marked influence on the assessment of the probability that concentration levels exceed a given threshold at locations downstream of a source of contamination. This element has also implications to the assessment of risk under uncertainty, as considering a Gaussian model for the log-conductivity



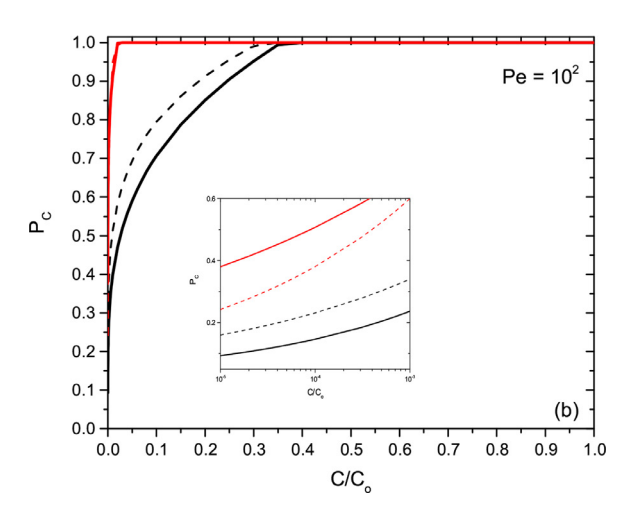


Fig. 6. Concentration CDF at the average plume displacement for two dimensionless times and selected values of Pe and α .

field clearly underestimates risk for distances close to the solute source zone (see Fig. 7). Our results show that the sensitivity to α of the probability of exceedance is strongest at early times and short distances from the source.

Finally, we compare the results for the concentration CDF obtained from Eq. (21) with the beta distribution. Several works have shown that such a distribution can be effectively employed as a proxy to estimate uncertainty associated with solute resident concentration in Gaussian random fields [13–15,22,53,58]. These authors appraise the accuracy of the beta distribution model by testing it against numerical simulations, analytical solutions and field data. Here, we analyze the ability of the beta distribution to approximate the uncertainty of the concentration in a non-Gaussian random field characterized through the GSG model. The beta CDF is given by:

$$P_{C}(c) = \frac{\Gamma[q_1 + q_2]}{\Gamma[q_1]\Gamma[q_2]} \int_0^c w^{q_1 - 1} (1 - w)^{q_2 - 1} dw, \tag{22}$$

where $\Gamma[z]$ is the Gamma function:

$$\Gamma[z] = \int_0^\infty \zeta^{z-1} e^{-\zeta} d\zeta, \qquad (23)$$

and

$$q_1 = \frac{\langle c \rangle}{\beta}; q_2 = \frac{1 - \langle c \rangle}{\beta}; \beta = \frac{\sigma_c^2}{\langle c \rangle (1 - \langle c \rangle) - \sigma_c^2}.$$
 (24)

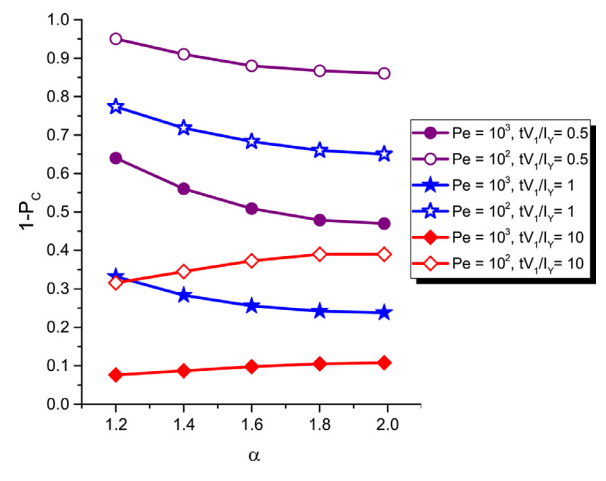


Fig. 7. Probability that concentration levels exceed the normalized threshold $c^* = 10^{-3}$ as a function of α and the Péclet number. Results are depicted for $\mathbf{x}/l_Y = (0.5, 0)^T$ and $tV_1/l_Y = 0.5$; $\mathbf{x}/l_Y = (1, 0)^T$ and $tV_1/l_Y = 1$; and $\mathbf{x}/l_Y = (10, 0)^T$ and $tV_1/l_Y = 10$.

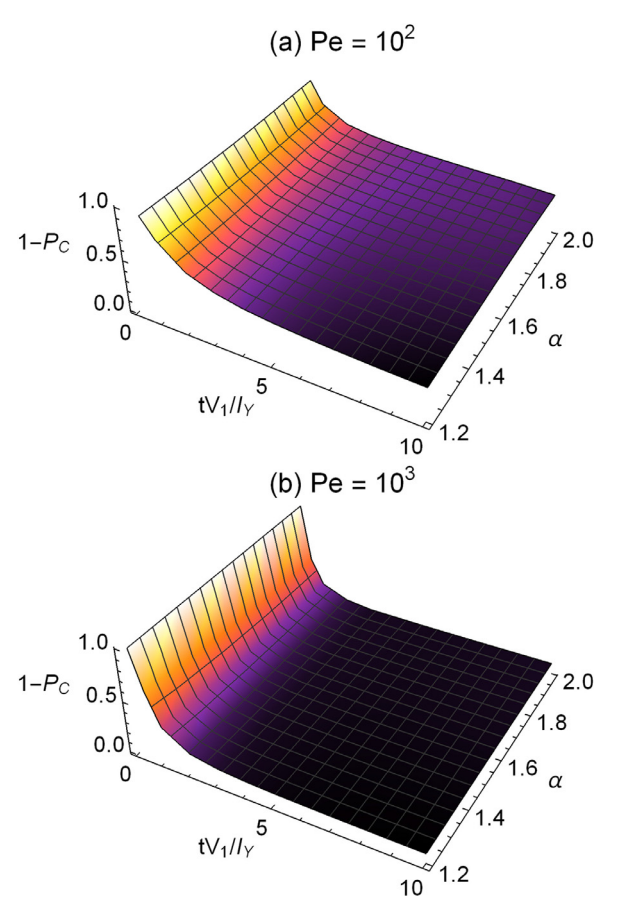
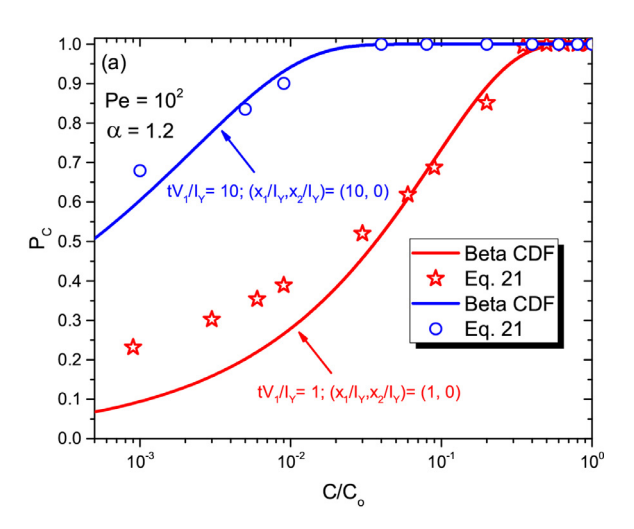


Fig. 8. Probability of exceedance of normalized concentration threshold $c^*=10^{-3}$ at the solute plume centroid position as a function of dimensionless time and α . Results are shown for Pe = (a) 10^2 and (b) 10^3 .

Fig. 9 depicts the concentration CDFs along the average plume displacement at two observation times for $Pe = 10^2$ and $\alpha = 1.2$ and $\alpha \to 2.0$. The results suggest that there is an overall good agreement between the CDF values obtained by Eq. (21) and the beta distribution (22) (as parametrized by the mean and variance of c, see Eqs. (11) and (12)). Consistent with the results reported in de Barros and Fiori [22], a mismatch between the beta distribution and Eq. (21) is documented at early times and at the lower



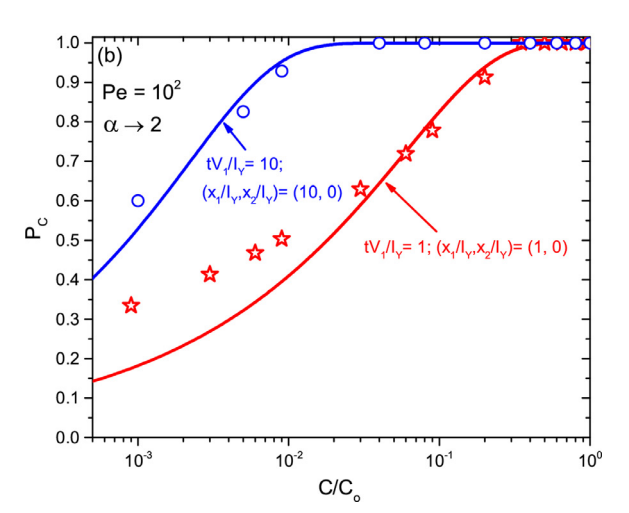


Fig. 9. Comparison between the concentration CDF model rendered by Eq. (21) and the β distribution, Eq. (22). Results are illustrated for Pe = 10^2 , (a) $\alpha = 1.2$ and (b) $\alpha \to 2$ at early and late times.

probability tails of the CDFs, where the beta distribution underestimates the probability that the concentration is lower than a given value. By way of example, when considering the concentration CDF at $tV_1/I_Y=1$ and $\mathbf{x}/I_Y=(1,0)^T$ for $\alpha=1.2$ (see Fig. 9a), one can note that the probability that the normalized concentration is lower than 0.01 is approximately equal to 0.27 for the beta CDF whereas the CDF given by Eq. (21) provides an approximate value of 0.4. On these bases, in the context of risk analysis one can view relying on the beta distribution as a worst case scenario, as compared to estimates provided by Eq. (21). For completeness, a comparison between the beta distribution and Eq. (21) are also illustrated for a Gaussian random log-conductivity field (Fig. 9b).

5. Conclusions

In this work we investigate the effects of non-Gaussianity in a random log-conductivity field, Y, on the statistics of the resident concentration c associated with a solute evolving in a randomly heterogeneous porous system. Through the use of a stochastic Lagrangian framework, we computed the mean, standard deviation and cumulative probabilistic distribution, CDF, of c at a given point in space and time for a 2D spatially heterogeneous (non-Gaussian) log-conductivity field. The Lagrangian framework utilized in our work has been successfully tested against field data and numer-

ical solutions (see [13,51,53]). Furthermore, we showed that the framework is capable of recovering previously published results for Gaussian *Y* fields. The effects of non-Gaussianity are incorporated in our study upon resting on the Generalized Sub-Gaussian model introduced by Riva et al. [41]. Our work leads to the following major conclusions:

- 1. The peak of the spatial distribution of the mean concentration increases as *Y* departs from Gaussianity. A similar behavior has been observed for the maximum value of the variance and for the minimum value of the coefficient of variation of *c*.
- 2. Differences between the statistics of *c* obtained within Gaussian and Generalized Sub-Gaussian Y fields decrease as travel time increases and as the Péclet number decreases.
- 3. Non-Gaussian effects are mainly manifested at the lower tail of the CDF of *c* at early times. We remark that these effects are relevant in probabilistic risk analysis, where exceedance of low concentration thresholds can be critical.
- 4. The beta distribution model can serve as a viable approximation for the concentration distribution in a non-Gaussian *Y*-field, its ability to capture the low probability tail of the CDF being otherwise limited. In addition, the beta distribution is fully characterized by the mean and standard deviation values. This implies that one can efficiently compute uncertainty estimates for the concentration at a given point in space and time. While the success of the beta distribution to represent uncertainty associated with *c* has been shown for Gaussian *Y* fields (e.g., see [15,22]), to the best of our knowledge, it is illustrated here for the first time for a non-Gaussian *Y* field.

The framework employed in this work can be viewed as an alternative to the numerical Monte Carlo method commonly used to estimate the uncertainty of a solute concentration. The approach here reported can also be used as a benchmark tool in computational stochastic mass transport problems in porous media. We remark that the results presented in this work are confined to small solute bodies (relative to the correlation length of the logconductivity random field), Y fields displaying low-to-mild heterogeneity, and 2D settings. A comparison between the system behavior in 2D and 3D settings for Gaussian flow fields is provided by de Barros and Fiori [22]. These authors show that solute concentration statistics are affected by flow dimensionality. Expanding the current framework to 3D settings is a topic of future work. Additional future research works will focus on the characterization of the effects of enhanced Y heterogeneity on the uncertainty of solute concentrations.

Declaration of Competing Interest

The authors declare that they have no known competing financial interests or personal relationships that could have appeared to influence the work reported in this paper.

CRediT authorship contribution statement

Felipe P.J. de Barros: Conceptualization, Formal analysis, Funding acquisition, Investigation, Methodology, Software, Validation, Visualization, Writing – original draft, Writing – review & editing. **Alberto Guadagnini:** Conceptualization, Formal analysis, Investigation, Methodology, Writing – original draft, Writing – review & editing. **Monica Riva:** Conceptualization, Formal analysis, Investigation, Methodology, Writing – original draft, Writing – review & editing.

Acknowledgments

The first author (F.P.J. de Barros) acknowledges the financial support provided by the National Science Foundation Grant num-

ber 1654009 and the Politecnico di Milano (Italy). Part of the research was developed while F.P.J. de Barros was visiting Professor at Politecnico di Milano.

Appendix A. Particle trajectory covariances

Semi-analytical expressions for the one- and two-particle trajectory covariances are here included under the assumptions adopted within this work (see Section 3). The complete set of details regarding the derivations of the particle trajectory functions are given, e.g., in Rubin [3], Fiori and Dagan [7], de Barros et al. [59].

The one particle trajectory covariance is given by

$$X_{ij}(t) = \frac{1}{2\pi} \int_0^t \int_0^t \int_{\mathbf{k}} \hat{v}_{ij}(\mathbf{k}) \cos[k_1 V_1(t'-t'')] e^{k^2 D|t'-t''|} dt' dt'' d\mathbf{k}.$$
(A.1)

which can be further simplified with the aid of the Cauchy algorithm, i.e. $\int_0^t \int_0^t h(|\tau-\tau'|)d\tau d\tau' = 2\int_0^t (t-\tau)h(\tau)d\tau$ with h representing a generic function. Therefore, Eq. (A.1) can be reduced to

$$X_{ij}(t) = \frac{4}{\pi} \int_0^t \int_0^\infty \hat{\nu}_{ij}(\mathbf{k}) \cos[k_1 V_1 \tau] e^{k^2 D \tau} d\tau d\mathbf{k}. \tag{A.2}$$

The two-particle trajectory covariance Z_{ij} is given by

$$Z_{ij}(t|\mathbf{a} - \mathbf{b}) = \frac{1}{2\pi} \int_0^t \int_0^t \int_{\mathbf{k}} \hat{v}_{ij}(\mathbf{k}) \psi(t', t'', \mathbf{k}|\mathbf{a} - \mathbf{b}) d\mathbf{k} dt' dt''$$
(A.3)

with

$$\psi(t', t'', \mathbf{k}|\mathbf{a} - \mathbf{b}) = e^{i\mathbf{k}\cdot(\mathbf{a} - \mathbf{b})}e^{-i\mathbf{k}\cdot\mathbf{V}(t' - t'')}e^{-k^2D(t' + t'')}$$
(A.4)

For a small injection zone, i.e. $\ell_i < I_Y$ (with i = 1, 2)

$$\lim_{\mathbf{a} \to \mathbf{b}} \psi(t', t'', \mathbf{k} | \mathbf{a} - \mathbf{b}) = e^{-\iota k_1 V_1(t' - t'')} e^{-k^2 D(t' + t'')}. \tag{A.5}$$

Substituting Eq. (A.5) into (A.3), yields the following integral expression for a 2D uniform-in-the-mean flow

$$Z_{ij}(t|\mathbf{a} - \mathbf{b}) = \frac{1}{2\pi} \int_0^t \int_0^t \int_{\mathbf{k}} \hat{v}_{ij}(\mathbf{k}) \cos[k_1 V_1(t' - t'')]$$

$$e^{-k^2 D(t' + t'')} d\mathbf{k} dt' dt''. \tag{A.6}$$

References

- [1] M. Moroni, J.H. Cushman, Statistical mechanics with three-dimensional particle tracking velocimetry experiments in the study of anomalous dispersion. II. Experiments, Phys. Fluids 13 (1) (2001) 81–91.
- [2] B. Berkowitz, H. Scher, Anomalous transport in correlated velocity fields, Phys. Rev. E 81 (1) (2010) 011128.
- [3] Y. Rubin, Applied Stochastic Hydrogeology, Oxford University Press, 2003.
- [4] J.G. Georgiadis, On the approximate solution of non-deterministic heat and mass transport problems, Int. J. Heat Mass Transf. 34 (8) (1991) 2097–2105.
- [5] Y. Rubin, M.A. Cushey, A. Bellin, Modeling of transport in groundwater for environmental risk assessment, Stoch. Hydrol. Hydraul. 8 (1) (1994) 57–77.
- [6] V. Kapoor, P.K. Kitanidis, Concentration fluctuations and dilution in aquifers, Water Resour. Res. 34 (5) (1998) 1181–1193.
- [7] A. Fiori, G. Dagan, Concentration fluctuations in aquifer transport: arigorous first-order solution and applications, J. Contam. Hydrol. 45 (1–2) (2000) 139–163.
- [8] D. Tonina, A. Bellin, Effects of pore-scale dispersion, degree of heterogeneity, sampling size, and source volume on the concentration moments of conservative solutes in heterogeneous formations, Adv. Water Resour. 31 (2) (2008) 339–354.
- [9] V. Kapoor, P.K. Kitanidis, Concentration fluctuations and dilution in two-dimensionally periodic heterogeneous porous media, Transp. Porous Media 22 (1) (1996) 91–119.
- [10] E. Morales-Casique, S.P. Neuman, A. Guadagnini, Non-local and localized analyses of non-reactive solute transport in bounded randomly heterogeneous porous media: theoretical framework, Adv. Water Resour. 29 (8) (2006) 1238–1255.
- [11] P.C. Chatwin, D.M. Lewis, P.J. Sullivan, Turbulent dispersion and the beta distribution, Environmetrics 6 (4) (1995) 395–402.

- [12] R.J. Munro, P.C. Chatwin, N. Mole, A concentration PDF for the relative dispersion of a contaminant plume in the atmosphere, Boundary-Layer Meteorol. 106 (3) (2003) 411–436.
- [13] A. Fiori, The Lagrangian concentration approach for determining dilution in aquifer transport: theoretical analysis and comparison with field experiments, Water Resour. Res. 37 (12) (2001) 3105–3114.
- [14] V. Fiorotto, E. Caroni, Solute concentration statistics in heterogeneous aquifers for finite Peclet values, Transp. Porous Med. 48 (3) (2002) 331–351.
- [15] A. Bellin, D. Tonina, Probability density function of non-reactive solute concentration in heterogeneous porous formations, J. Contam. Hydrol. 94 (1–2) (2007) 109–125.
- [16] O.A. Cirpka, R.L. Schwede, J. Luo, M. Dentz, Concentration statistics for mixing-controlled reactive transport in random heterogeneous media, J. Contam. Hydrol. 98 (1–2) (2008) 61–74.
- [17] D.W. Meyer, P. Jenny, H.A. Tchelepi, A joint velocity-concentration PDF method for tracer flow in heterogeneous porous media, Water Resour. Res. 46 (12) (2010) W12522, doi:10.1029/2010WR009450.
- [18] M. Shvidler, K. Karasaki, Probability density functions for solute transport in random field, Transp. Porous Med. 50 (3) (2003) 243–266.
- [19] X. Sanchez-Vila, A. Guadagnini, D. Fernandez-Garcia, Conditional probability density functions of concentrations for mixing-controlled reactive transport in heterogeneous aquifers, Math. Geosci. 41 (3) (2009) 323–351.
 [20] M. Dentz, D.M. Tartakovsky, Probability density functions for passive scalars
- [20] M. Dentz, D.M. Tartakovsky, Probability density functions for passive scalars dispersed in random velocity fields, Geophys. Res. Lett. 37 (24) (2010) L24406, doi:10.1029/2010GL045748.
- [21] O.A. Cirpka, F.P.J. de Barros, G. Chiogna, W. Nowak, Probability density function of steady state concentration in two-dimensional heterogeneous porous media, Water Resour. Res. 47 (11) (2011) W11523, doi:10.1029/2011WR010750.
- [22] F.P.J. de Barros, A. Fiori, First-order based cumulative distribution function for solute concentration in heterogeneous aquifers: theoretical analysis and implications for human health risk assessment, Water Resour. Res. 50 (5) (2014) 4018–4037
- [23] F. Boso, S.V. Broyda, D.M. Tartakovsky, Cumulative distribution function solutions of advection-reaction equations with uncertain parameters, Proc. R. Soc. A 470 (2166) (2014) 20140189.
- [24] J.J. Gómez-Hernández, X.-H. Wen, To be or not to be multi-Gaussian? A reflection on stochastic hydrogeology, Adv. Water Resour. 21 (1) (1998) 47–61.
- [25] C.P. Haslauer, P. Guthke, A. Bárdossy, E.A. Sudicky, Effects of non-Gaussian copula-based hydraulic conductivity fields on macrodispersion, Water Resour. Res. 48 (7) (2012) W07507, doi:10.1029/2011WR011425.
- [26] C.B. Rizzo, F.P.J. de Barros, Minimum hydraulic resistance and least resistance path in heterogeneous porous media, Water Resour. Res. 53 (10) (2017) 8596–8613.
- [27] A. Guadagnini, M. Riva, S.P. Neuman, Recent advances in scalable non-Gaussiangeostatistics: the generalized sub-Gaussian model, J. Hydrol. 562 (2018) 685–691.
- [28] R. Benzi, S. Ciliberto, R. Tripiccione, C. Baudet, F. Massaioli, S. Succi, Extended self-similarity in turbulent flows, Phys. Rev. E 48 (1) (1993) R29.
- [29] S. Chakraborty, U. Frisch, S.S. Ray, Extended self-similarity works for the burgers equation and why, J. Fluid Mech. 649 (2010) 275285.
- [30] M. Siena, A. Guadagnini, M. Riva, S.P. Neuman, Extended power-law scaling of air permeabilities measured on a block of tuff, Hydrol. Earth Syst. Sci. 16 (1) (2012) 29.
- [31] S. Painter, Evidence for non-Gaussian scaling behavior in heterogeneous sedimentary formations, Water Resour. Res. 32 (5) (1996) 1183–1195.
- [32] H.H. Liu, F.J. Molz, Comment on evidence for non-Gaussian scaling behavior in heterogeneous sedimentary formations by scott painter, Water Resour. Res. 33 (4) (1997) 907–908.
- [33] M.M. Meerschaert, T.J. Kozubowski, F.J. Molz, S. Lu, Fractional laplace model for hydraulic conductivity, Geophys. Res. Lett. 31 (8) (2004) L08501, doi:10.1029/ 2003GL019320.
- [34] M. Siena, M. Riva, M. Giamberini, P. Gouze, A. Guadagnini, Statistical modeling of gas-permeability spatial variability along a limestone core, Spat. Stat. 34 (2019) 100249.
- [35] M. Riva, S.P. Neuman, A. Guadagnini, Sub-Gaussian model of processes with heavy-tailed distributions applied to air permeabilities of fractured tuff, Stoch. Environ. Res. Risk Assess. 27 (1) (2013) 195–207.

- [36] M. Riva, S.P. Neuman, A. Guadagnini, M. Siena, Anisotropic scaling of berea sandstone log air permeability statistics, Vadose Zone J. 12 (3) (2013) 1–15.
- [37] Y. Hyun, Multiscale Anaylses of Permeability in Porous and Fractured Media, 2002 Ph.D. dissertation.
- [38] S. Painter, Flexible scaling model for use in random field simulation of hydraulic conductivity, Water Resour. Res. 37 (5) (2001) 1155–1163, doi:10.1029/ 2000WR900394.
- [39] C.-Y. Yang, K.-C. Hsu, K.-C. Chen, The use of the levy-stable distribution for geophysical data analysis, Hydrogeol. J. 17 (5) (2009) 1265–1273.
- [40] A. Guadagnini, S.P. Neuman, M.G. Schaap, M. Riva, Anisotropic statistical scaling of soil and sediment texture in a stratified deep vadose zone near Maricopa, Arizona, Geoderma 214 (2014) 217–227.
- [41] M. Riva, S.P. Neuman, A. Guadagnini, New scaling model for variables and increments with heavy-tailed distributions, Water Resour. Res. 51 (6) (2015) 4623–4634
- [42] V. Ganti, A. Singh, P. Passalacqua, E. Foufoula-Georgiou, Subordinated Brownian motion model for sediment transport, Phys. Rev. E 80 (1) (2009) 011111.
- [43] M. Siena, A. Guadagnini, A. Bouissonnie, P. Ackerer, D. Daval, M. Riva, Generalized sub-Gaussian processes: theory and application to hydrogeological and geochemical data, Water Resour. Res. (2020). e2020WR027436
- [44] M. Riva, M. Panzeri, A. Guadagnini, S.P. Neuman, Simulation and analysis of scalable non-Gaussianstatistically anisotropic random functions, J. Hydrol. 531 (2015) 88–95.
- [45] M. Riva, A. Guadagnini, S.P. Neuman, Theoretical analysis of non-Gaussian heterogeneity effects on subsurface flow and transport, Water Resour. Res. 53 (4) (2017) 2998–3012.
- [46] A. Libera, F.P.J. de Barros, M. Riva, A. Guadagnini, Solute concentration at a well in non-Gaussianaquifers under constant and time-varying pumping schedule, J. Contam. Hydrol. 205 (2017) 37–46.
- [47] F.P.J. de Barros, M.J. Colbrook, A.S. Fokas, A hybrid analytical-numerical method for solving advection-dispersion problems on a half-line, Int. J. Heat Mass Transf. 139 (2019) 482–491.
- [48] G. Hwang, A unified approach to two-dimensional linear advection-dispersion equation in cylindrical coordinates on a finite domain, Int. J. Heat Mass Transf. 164 (2021) 120569.
- [49] L.W. Gelhar, C.L. Axness, Three-dimensional stochastic analysis of macrodispersion in aquifers, Water Resour. Res. 19 (1) (1983) 161–180.
- [50] G. Dagan, Solute transport in heterogeneous porous formations, J. Fluid Mech. 145 (1984) 151–177.
- [51] F.P.J. de Barros, A. Fiori, F. Boso, A. Bellin, A theoretical framework for modeling dilution enhancement of non-reactive solutes in heterogeneous porous media, J. Contam. Hydrol. 175 (2015) 72–83.
- [52] M.R. Soltanian, F. Behzadi, F.P.J. de Barros, Dilution enhancement in hierarchical and multiscale heterogeneous sediments, J. Hydrol. 587 (2020) 125025.
- [53] F. Boso, F.P.J. de Barros, A. Fiori, A. Bellin, Performance analysis of statistical spatial measures for contaminant plume characterization toward risk-based decision making, Water Resour. Res. 49 (6) (2013) 3119–3132.
- [54] A.M. Mood, F.A. Graybill, D.C. Boes, Introduction to the Theory of Statistics, third ed., McGraw Hill, 1973.
- [55] M. Riva, M. Willmann, Impact of log-transmissivity variogram structure on groundwater flow and transport predictions, Adv. Water Resour. 32 (8) (2009) 1311–1322.
- [56] A. Fiori, G. Dagan, Concentration fluctuations in transport by groundwater: comparison between theory and field experiments, Water Resour. Res. 35 (1) (1999) 105–112.
- [57] G. Sole-Mari, M. Riva, D. Fernàndez-Garcia, X. Sanchez-Vila, A. Guadagnini, Solute transport in bounded porous media characterized by generalized sub-Gaussian log-conductivity distributions, Adv. Water Resour. 147 (2021) 103812.
- [58] A. Bonazzi, M. Morvillo, J. Im, B. Jha, F.P.J. de Barros, Relative impacts of permeability heterogeneity and viscosity contrast on solute mixing, Physical Review Fluids 6 (6) (2021) 064501, doi:10.1103/PhysRevFluids.6.064501.
- [59] F.P.J. de Barros, A. Fiori, A. Bellin, A simple closed-form solution for assessing concentration uncertainty, Water Resour. Res. 47 (12) (2011) W12603, doi:10. 1029/2011WR011107.